J. Fluid Mech. (1988), *vol.* 193, *pp.* 27–51
Printed in Great Britain

On shear layers in mixture separation in rotating containers with inclined walls

By M. UNGARISH
Computer Science Department, Technion, Haifa 32000, Israel

(Received 19 February 1987 and in revised form 12 October 1987)

The rotating flow of a separating mixture within an axisymmetric container is considered with emphasis on the pure fluid layer adjacent to the inclined 'bottom' boundary from which particles are removed by centrifugal buoyancy. Within the framework of 'mixture' ('diffusion') model and when the relative density difference, the Ekman number E and particle Taylor number β are small, it is shown that the behaviour of that layer is governed by $\Xi = E^{\frac{1}{3}}\alpha_1|\cot\gamma^B|/\beta$ (where α_1 is the volume fraction of the dispersed particles and γ^B is the elevation angle of the bottom wall with respect to the centrifugal force). If Ξ is small the layer thickens quickly into an inviscid core, in accordance with previous studies. However, novel features show up for Ξ large or $O(1)$, when the viscosity-induced Ekman suction is able to counteract the separation velocity. In the former case the pure fluid layer is thin and quasi-steady, and the remaining part of the interface is essentially perpendicular to the force field, in close apparent resemblance to the analog gravitational process. In the latter case, a thin quasi-steady layer and a continuously thickening core of pure fluid coexist in the same vessel.

1. Introduction

The separation of a two-phase mixture in a force field is a fascinating process with a large variety of industrial applications. Of particular interest is the settling in large (as compared to the typical width of boundary and sediment layers) containers with walls inclined with respect to the field. Gravitational sedimentation in such vessels is often enhanced by a special convective phenomenon, the 'Boycott effect'. Although known to fluid dynamicists for more than 60 years, this effect has been satisfactorily understood and the corresponding flow field has been properly analysed only recently, in particular by Acrivos & Herbolzheimer (1979) and Schneider (1982). The most striking result concerns the shape and motion of the interface between the clean fluid and the mixture. First, the pure fluid layer beneath the downward-inclined wall is thin and essentially steady, see section AB in figure 1. Second, the remaining part of the interface, i.e. section BC in figure 1, is effectively horizontal and falls with a vertical velocity considerably greater than in a similar non-inclined vessel. Acrivos & Herbolzheimer (1979) studied the pure fluid layer dominated by a viscous–buoyancy balance and Schneider's (1982) investigation focused on a convection–buoyancy equilibrium.

This remarkably simple shape of the interface facilitates the straightforward calculation of the volumetric sedimentation rate dV_D^*/dt^* and of the dh^*/dt^* by explicit formulae usually referred to as the PNK (Ponder–Nakamura–Kuroda) theory, cf. Appendix B. For the configuration in figure 1 it essentially asserts that dV_D^*/dt^* is proportional to the instantaneously horizontal projection $\overline{AC'}$ and

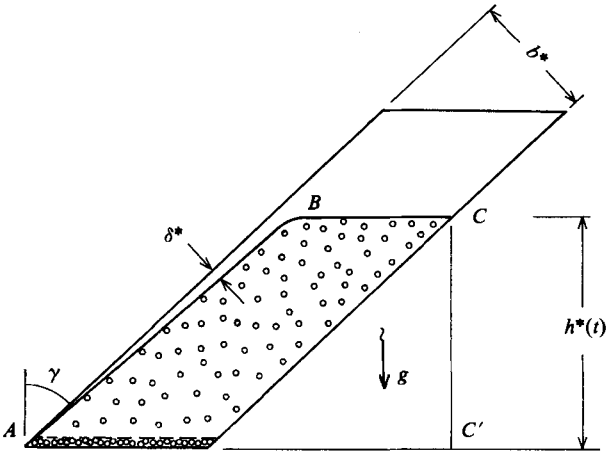

FIGURE 1. Gravitational settling of heavy particle mixture in inclined tanks.

$\mathrm{d}h^*/\mathrm{d}t^*$ is augmented by a factor of $(\overline{AC'}/\overline{BC})$ as compared to the uninclined vessel.

The understanding of the centrifugal separation in a geometrically similar device is obviously of great significance. However, very little was done on this topic until quite recently, probably because of difficulties in both experimentation and theory of rotating two-phase flows.

The paper of Greenspan & Ungarish (1985*a*) considered this problem under assumptions similar to those of Acrivos & Herbolzheimer (1979) and of Schneider (1982), i.e. that inertial and viscous effects are negligibly small in the main mixture core and the relative (slip) velocity between the phases is parallel to the buoyancy force (see discussion following (2.1*b*)). It argued that the Coriolis forces may induce a flow pattern surprisingly different from the gravitational one. In axisymmetric containers these forces dominate the motion in the core and, consequently: (*a*) the radial velocity of that portion of interface perpendicular to the centrifugal force cannot be augmented as compared to the settling in a straight container; (*b*) the pure fluid layer, formed on the inclined wall from which particles are removed by the buoyancy force, is time dependent and thickens considerably during the process. On the other hand, in a sectioned rotating container, where the azimuthal motion is blocked, the Coriolis terms are less significant and the flow bears more similarity to the gravitational case. The qualitative results have been essentially confirmed by experiments. Amberg & Greenspan (1987).

Subsequently, Greenspan & Ungarish (1985*b*) quantitatively analysed the flow field and the motion of the interface in the axisymmetric case assuming that the pure fluid and the mixture are inviscid bulks matched by fully developed Ekman layers. They indicated that these bulks possess considerable rotation (the heavier one retrograde respective to the container and vice versa) and that the separating interface is not perpendicular to the centrifugal force. The centrifugal analog of the PNK theory (cf. Appendix B) is not valid in these circumstances.

The present paper studies additional aspects of the two-phase viscous rotating shear layers and their implications on the velocity field and on the shape and motion of the interface in an axisymmetric container. In particular, it reveals the significance of the parameter $\Xi = (E^{\frac{1}{2}}\alpha_{\mathrm{I}}|\cot\gamma^{\mathrm{B}}|/\beta)$, where E is the Ekman number and β is the

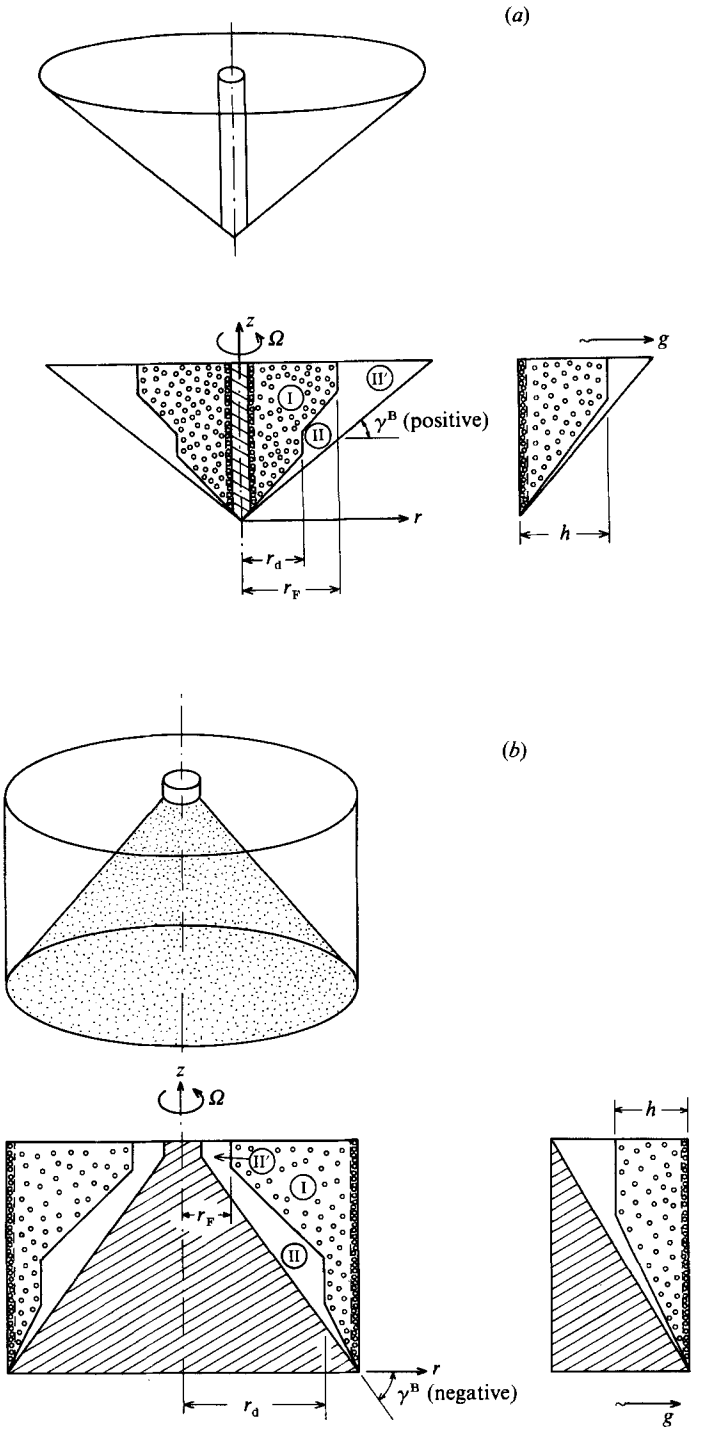

FIGURE 2. Schematic description of centrifugal separation in conical container, and analog process in gravity (*a*) light particles; (*b*) heavy particles.

(modified) Taylor number of the particle, both defined in §2, α_I is the dispersed volume fraction in the mixture and γ^B is the elevation angle of the wall from which particles are removed with respect to the centrifugal force. If this parameter is small, the inviscid bulk motion described by Greenspan & Ungarish (1985*b*) prevails. For large values of Ξ, however, the viscous forces become more pronounced and the pure fluid layer adjacent to an inclined boundary remains thin and quasi-steady, while the remaining portion of the interface is essentially perpendicular to the centrifugal force. In this case the appropriate modification of the PNK theory can be applied. When Ξ is of order unity, both a thin viscous quasi-steady layer and a thick inviscid time dependent core of pure fluid show up in the same container, cf. figure 2. In any case, the thickness of the quasi-steady pure fluid layer cannot exceed $\pi(\mu_c^*/\rho_c^* \Omega^* \cos\gamma^B)^{\frac{1}{2}}$ where Ω^* is the angular velocity of the container, μ_c^* and ρ_c^* are the viscosity and density of the fluid.

These predictions have been tentatively confirmed by experiments with the separation of light particles in a conical transparent container (Greenspan, private communication). Values of $\Xi \sim 0.8$–1.5 were obtained in a system essentially similar to that used by Amberg & Greenspan (1987), where $\Xi \sim 0.05$. The presence of a thin pure fluid layer for the larger values of Ξ only was clearly observed. At this time there is insufficient information for a more significant and quantitative comparison.

A particular configuration of the present theory, not elaborated here, concerns separation in a container whose top and bottom walls are parallel conical disks. This case is closely related to the study of Amberg *et al.* (1986). However, these authors restricted their analysis to narrow disk spacings and, implicitly, to small values of Ξ.† Under these circumstances, batch separation is completed in a much smaller time interval than the one considered here. Therefore, Amberg *et al.* focused attention on the time dependent growth of the Ekman layers which are regarded as quasi-steady in the present paper. Nevertheless, the results of both investigations are consistent in the domain where overlapping is expected.

2. Formulation

Consider the time-dependent motion of a mixture of two incompressible constituents. The dispersed phase consists of small particles (or droplets) of approximately constant radius a^* and occupies the volume fraction α. The averaged flow variables of the continuous and dispersed phase are denoted by subscripts C and D, while a variable of the mixture is unsubscripted with the exception $\alpha \equiv \alpha_D$ (e.g. the densities, ρ_D^*, ρ_C^* and $\rho^* = (1-\alpha)\rho_C^* + \alpha\rho_D^*$). A superscript asterisk designates a dimensional variable.

The cylindrical coordinate system (r, θ, z) is attached to the container rotating with $\Omega^* \hat{z}$, cf. figure 3. The outer radius of the tank, r_o^*, is used as a reference length, and $z^T(r)$, $z^B(r)$ and r_i define the top, bottom and inner solid boundaries.

Special interest will be focused on the flow in the proximity of the top, bottom and interface surfaces, designated respectively by upper index T, B and Σ, when necessary. To each one, local boundary-layer coordinates $(\xi, \theta, \delta\zeta)$ are attached as specified in §4. In general, the unit vectors, $\hat{n}$, normal to the axisymmetric surfaces

† Two major parameters of Amberg *et al.* are, in the original notation, the gap Taylor number, T, and the reduced boundary-layer volume flux, ϵ, which turns out to bear the features of the present Ξ. The present theory deals with $T > (2\pi)^2$ and $\Xi > 1$, while Amberg *et al.* are mainly concerned with smaller values of these parameters, especially of the latter one. In addition, these authors investigated a continuous settling process which is irrelevant here.

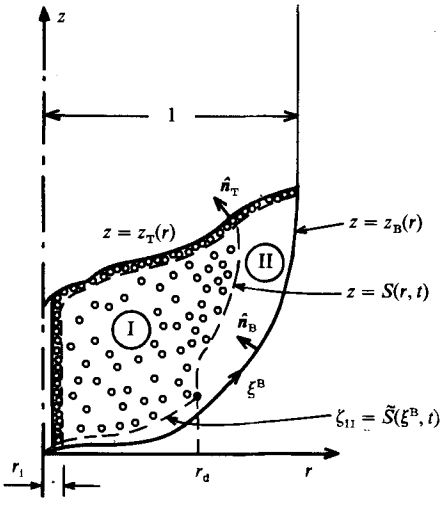

FIGURE 3. Illustration of geometrical definitions.

are defined as pointing upwards, i.e. $\hat{\boldsymbol{n}}\cdot\hat{\boldsymbol{z}} > 0$ always. The appropriate inclination is designated by the sharp angle $\gamma = -\sin^{-1}(\hat{\boldsymbol{n}}\cdot\hat{\boldsymbol{r}})$, $-\frac{1}{2}\pi \leqslant \gamma \leqslant \frac{1}{2}\pi$, which is positive for inwardly tilted surfaces and conversely, as inferred from figure 2.

To accommodate the analysis to both heavy and light dispersions, it is convenient to require that the buoyancy pushes away particles from the bottom wall. In other words, $\gamma^B > 0$ for heavy particles and vice versa. The top boundary either collects particles or is parallel to the force field, $\gamma^T = 0$.

Let $\boldsymbol{q}^* = (\alpha\rho_D^*\boldsymbol{q}_D^* + (1-\alpha)\rho_C^*\boldsymbol{q}_C^*)/\rho^*$ be the mixture mass velocity and let $\boldsymbol{j}^* = \alpha\boldsymbol{q}_D^* + (1-\alpha)\boldsymbol{q}_C^*$ be the corresponding volume flux. The components of $\boldsymbol{q}^*$ in the (r, θ, z) system are u^*, v^*, w^*. The primary variable of the process under investigation is the relative velocity, $\boldsymbol{q}_R^*(= \boldsymbol{q}_D^* - \boldsymbol{q}_C^*)$,† which is subsequently approximated by

$$\boldsymbol{q}_R^* = \epsilon\beta(1-\alpha)\frac{1}{\mu(\alpha)}\Omega^* r^* \hat{\boldsymbol{r}}, \tag{2.1}$$

where

$$\epsilon = \frac{\rho_D^* - \rho_C^*}{\rho_C^*}, \tag{2.2a}$$

$$\beta = \frac{2}{9}\frac{a^{*2}}{(\mu_C^*/\Omega^*\rho_C^*)}, \tag{2.2b}$$

is the particle Taylor number and $\mu(\alpha)$ is the ratio of the effective viscosity of the mixture to that of the clear continuous fluid, μ_C^*, to be specified below. Equation (2.1) reflects the balance between centrifugal buoyancy and Stokes drag on the particle. This balance may be considerably affected by Coriolis forces when β is not small, see Ungarish & Greenspan (1984*b*), figure 2. (Note that this parameter measures the ratio of the particle size to the thickness of the Ekman layer, or equivalently the ratio of the Coriolis force and Stokes drag on a particle. Thus, while the Coriolis terms are essential in the flow field balances, they are considered as unimportant in the local

† Several useful kinematic relationships between velocities and fluxes are given in Appendix A.

motion of the dispersed particle relative to the fluid.) However, the subsequent analysis of the Ekman layers strongly relies on a^* being small compared to the typical thickness $(\mu_C^*/\rho_C^* \Omega^*)^{\frac{1}{2}}$. This requirement obviously implies $\beta \ll 1$ which vindicates the employment of (2.1). The leading features of $\mu(\alpha)$ appear in the correlation derived by Ishii & Zuber (1979)

$$\mu(\alpha) = \left(1 - \frac{\alpha}{\alpha_M}\right)^{-2.5\alpha_M}, \tag{2.3}$$

where α_M is the maximal packing volume fraction. This particular choice, however, is not essential in what follows.

Introduce dimensionless variables obtained by scaling the lengths by r_o^* (the outer radius of the container), velocities by $|\epsilon|\beta\Omega^* r_o^*$ (the typical value of q_R^*), time by $(|\epsilon|\beta\Omega)^{-1}$ (the timescale of radial separation), density by ρ_C^* and the pressure by $\rho_C^*|\epsilon|(\Omega r_o^*)^2$. The equations of continuity are

$$\frac{\partial \alpha}{\partial t} + \nabla \cdot \alpha \boldsymbol{q}_D = 0, \tag{2.4}$$

$$\nabla \cdot \boldsymbol{j} = 0. \tag{2.5}$$

The rotational accleration terms are readily incorporated in the momentum equations of the mixture as developed, for instance, by Ishii (1975, chapter 10), and the stress term is assumed to be that of a Newtonian fluid. In dimensionless form this reads

$$(1+\epsilon\alpha)\left\{2\hat{z} \times \boldsymbol{q} + |\epsilon|\beta\left[\frac{\partial \boldsymbol{q}}{\partial t} + \tfrac{1}{2}\nabla(\boldsymbol{q}\cdot\boldsymbol{q}) + (\nabla \times \boldsymbol{q}) \times \boldsymbol{q}\right]\right\}$$
$$= -\frac{1}{\beta}\nabla p + \frac{s}{\beta}\alpha r\hat{\boldsymbol{r}} - E\mu(\alpha)\left[\nabla \times \nabla \times \boldsymbol{q} - (\tfrac{4}{3})\nabla(\nabla \cdot \boldsymbol{q})\right] - |\epsilon|\beta\nabla \cdot \left[\alpha(1-\alpha)\frac{1+\epsilon}{1+\epsilon\alpha}\boldsymbol{q}_R \boldsymbol{q}_R\right], \tag{2.6}$$

where p is the reduced pressure,

$$s = \epsilon/|\epsilon|, \tag{2.7a}$$

and

$$E = \frac{\mu_C^*}{\rho_C^* \Omega^* r_o^{*2}} \tag{2.7b}$$

is the Ekman number. Gravity is neglected compared to the centrifugal acceleration. The last term in (2.6) arises from the diffusion of momentum due to the relative motion. Note that the equations (2.4)–(2.6) properly reduce to the pure fluid case when $\alpha = 0$.

Using the dimensionles form of (2.1),

$$\boldsymbol{q}_R = s[\mu(\alpha)]^{-1}(1-\alpha)\, r\hat{\boldsymbol{r}}, \tag{2.8}$$

and the kinematic relationship $\boldsymbol{q}_D = \boldsymbol{j} + (1-\alpha)\boldsymbol{q}_R$ the equations of continuity (2.4)–(2.5) give

$$\frac{\partial \alpha}{\partial t} + [\boldsymbol{j} + s\Phi'(\alpha)\, r\hat{\boldsymbol{r}}] \cdot \nabla\alpha = -2s\Phi(\alpha), \tag{2.9}$$

where

$$\Phi(\alpha) = \alpha(1-\alpha)^2/\mu(\alpha). \tag{2.10}$$

The apparent boundary conditions are: no slip and no penetration on the solid walls. The initial conditions are solid rotation (for simplicity) and $\alpha(r, t=0) = \alpha(0) =$ constant through the container.

The objective is to calculate $\boldsymbol{q}(\boldsymbol{r},t)$ and $\alpha(\boldsymbol{r},t)$ from the system (2.5)–(2.10) supplemented by the kinematic relationship (A 8) between $\boldsymbol{j}$ and $\boldsymbol{q}$ which for the present case yields

$$\boldsymbol{j} = \boldsymbol{q} - |\epsilon| \frac{\Phi(\alpha)}{1+\epsilon\alpha} r\hat{\boldsymbol{r}}. \tag{2.11}$$

In particular, attention is focused on the description of the shape and motion of the interface between the regions of mixture and pure fluid. This is a formidable task, and further simplifications are necessary for progress.

A major simplification is the linear flow obtained when the convective inertial terms in (2.6) are negligibly small. This limit represents a small deviation from solid rotation and can be shown to correspond to $|\epsilon| \ll 1$ (i.e. $|\epsilon|$ turns out to be the representative Rossby number). The diffusion of momentum represented by the last term in (2.6) is negligible as compared to the buoyancy term because β and $|\epsilon|$ are both small. Considering $E \ll 1$, the solution of the remaining system is facilitated by decomposing the present flow field into inviscid components and viscous 'corrections'. The latter are induced mainly by shear layers of Ekman type. However, this paper indicates that in a certain parameter range the 'vertical' $E^{\frac{1}{4}}$ and $E^{\frac{1}{3}}$ viscous regions may contribute significantly to the final flow pattern. It should be born in mind that the choice of reference velocity implies $\boldsymbol{q}_{\mathrm{R}} \cdot \hat{\boldsymbol{r}} = O(1)$, but the order of magnitude of the components of $\boldsymbol{q}$ turns out to be different; in particular, the azimuthal and axial velocities are $O(\alpha/\beta)$ and $O(E^{\frac{1}{3}}(\alpha/\beta))$.

If the motion is stable, the flow field is partitioned into three distinct regions (figure 3): the mixture, the pure fluid (formed adjacent to the bottom wall from which particles depart under the action of the centrifugal buoyancy force) and the sediment layer (formed on the opposite solid boundary). The first and second region are hereinafter referred to as I and II and the corresponding variables subscribed accordingly when necessary. In the subregion II′ of II the pure fluid occupies the entire axial interval between the top and bottom boundaries. This fluid apparently has a passive role in the separation process and will not be considered in detail.

The motion of the sediment is believed to be rather insignificant in the present configuration, provided that $(\alpha/\alpha_{\mathrm{M}})$ is fairly small. Consequently, boundary conditions for regions I and II are applied directly on the solid wall.

Obviously, $\alpha_{\mathrm{II}} = 0$. The value of α in region I is obtained via the solution of (2.9) along characteristic paths on which

$$\frac{\mathrm{d}\alpha_{\mathrm{I}}}{\Phi(\alpha_{\mathrm{I}})} = -2s\,\mathrm{d}t. \tag{2.12}$$

Since initially $\alpha_{\mathrm{I}} = \alpha(0) = \text{constant}$,it follows that (2.12) is valid in the entire region. Thus $\alpha_{\mathrm{I}} = \alpha_{\mathrm{I}}(t)$ can be calculated directly by (2.12).

The interface between regions I and II is regarded as a sharp discontinuity, a kinematic shock, described by the surface $\Sigma(\boldsymbol{r},t) = 0$ whose velocity in the rotating system is $\boldsymbol{q}_{\Sigma}$. It follows:

$$\frac{\partial \Sigma}{\partial t} + \boldsymbol{q}_{\Sigma} \cdot \boldsymbol{\nabla}\Sigma = 0. \tag{2.13}$$

The continuity of the dispersed component's flux $\alpha\boldsymbol{q}_{\mathrm{D}}$ across the interface implies

$$[\alpha(\boldsymbol{q}_{\mathrm{D}} - \boldsymbol{q}_{\Sigma})]^{+}_{-} \cdot \boldsymbol{\nabla}\Sigma = 0. \tag{2.14}$$

Here $+$ and $-$ denote the sides of the interface adjacent to regions I and II. Since $\alpha_{\mathrm{II}} = 0$ this gives:

$$\boldsymbol{q}_{\Sigma} \cdot \boldsymbol{\nabla}\Sigma = \boldsymbol{q}_{\mathrm{D_I}} \cdot \boldsymbol{\nabla}\Sigma. \tag{2.15}$$

Substituting (2.15) into (2.13) and using the kinematic relationship (A 3) and equations (2.8) and (2.10) yield the following useful equation of motion of the interface:

$$\frac{\partial \Sigma}{\partial t}+\left(\boldsymbol{q}_{\mathrm{I}}+s\frac{\Phi(\alpha_{\mathrm{I}})}{\alpha_{\mathrm{I}}}r\hat{\boldsymbol{r}}\right)\cdot\boldsymbol{\nabla}\Sigma=0, \tag{2.16}$$

subject to the condition that $\Sigma(\boldsymbol{r},t=0)$ coincides with the container's boundary.

3. The inviscid component

Consider the flow variables for $E=0$. When necessary, the resulting components are designated by the superscript 'inv'.

The appropriate linear momentum equations are

$$2\hat{\boldsymbol{z}}\times\boldsymbol{q}_{\mathrm{I}}=-\frac{1}{\beta}\boldsymbol{\nabla}p_{\mathrm{I}}+\frac{s}{\beta}\alpha_{\mathrm{I}}r\hat{\boldsymbol{r}}, \tag{3.1}$$

$$2\hat{\boldsymbol{z}}\times\boldsymbol{q}_{\mathrm{II}}=-\frac{1}{\beta}\boldsymbol{\nabla}p_{\mathrm{II}}. \tag{3.2}$$

The axial ($\hat{\boldsymbol{z}}$) component of these equations indicates that p_{I} and p_{II} are not functions of z. Moreover, since the viscous layers adjacent to the interface cannot support an axial pressure difference it is concluded that:

$$p_{\mathrm{I}}=p_{\mathrm{II}}=p(r,t). \tag{3.3}$$

The result of combining the last equation with the azimuthal component of (3.1)–(3.2) is:

$$v_{\mathrm{II}}=v_{\mathrm{I}}+\frac{s\alpha_{\mathrm{I}}(t)}{2\beta}r, \tag{3.4}$$

$$\frac{\partial v_{\mathrm{II}}}{\partial z}=\frac{\partial v_{\mathrm{I}}}{\partial z}=0. \tag{3.5}$$

In addition, (3.1)–(3.2) give

$$u_{\mathrm{I}}=u_{\mathrm{II}}=0. \tag{3.6}$$

A more rigorous analysis shows that actually $u_{\mathrm{I,II}}=O(\epsilon r)$. Equations (3.4)–(3.5) suggest the introduction of

$$v_{\mathrm{I,II}}=\frac{\alpha_{\mathrm{I}}(t)}{2\beta}r\omega_{\mathrm{I,II}}(r,t), \tag{3.7a}$$

with

$$\omega_{\mathrm{II}}=\omega_{\mathrm{I}}+s, \tag{3.7b}$$

where $\omega_{\mathrm{I,II}}$ are $O(1)$ variables.

Thus, to this order of approximation, the inviscid radial motion is zero, but a considerable inviscid angular velocity component $O(\alpha_{\mathrm{I}}/\beta)$, shows up.

These inviscid components dominate the velocity field in the cores of regions I, II, whose axial dimension is large compared to $E^{\frac{1}{2}}$. However, the determination of ω, the fulfilment of boundary conditions, the smoothing of the discontinuity $\omega_{\mathrm{I}}-\omega_{\mathrm{II}}$ across the interface, the calculation of the axial component w (which is critical to the motion of the interface) and the establishment of conditions under which the initially thin region II develops into a core require the analysis of the viscous corrections induced by the thin shear Ekman layers. This is performed in the next section.

4. The viscous Ekman layer 'corrections'

These shear layers form on or around the surface $z = \sigma(r)$ (top and bottom walls and interface). It is therefore convenient to analyse them in the boundary-layer coordinate system $[\xi, \theta, \delta\zeta]$ as sketched in figure 4. It is anticipated that $\delta = (\mu(\alpha)E)^{\frac{1}{2}}$. The curved coordinate $\xi = \xi(r)$ measures the distance from the axis of rotation along the intersection between the surface and the meridional plane $\theta =$ constant; ζ is in the same plane, perpendicular to ξ and pointing 'upwards'. The metric coefficients are, approximately: $1, r(\xi), \delta$. For additional details see Greenspan (1968, chapter 1.6).

Let γ be the local angle of inclination of the surface, $|\gamma| = -\sin^{-1}(\hat{\boldsymbol{r}}\cdot\hat{\boldsymbol{\zeta}})$, and denote by $(q_\xi, q_\theta, q_\zeta)$ the velocity components.

Boundary layer 'corrections', denoted by tildes, are added to the inviscid balance discussed in the preceding section. Note that $\tilde{\alpha} = 0$. Moreover, it is postulated that the relative velocity correlation (2.8) is unaffected by the strong shear in the present layers. Upon substituting in the quasi-steady† linear form of (2.5)–(2.6) and eliminating the 'inviscid' balance one gets, to leading order in E,

$$\frac{1}{r}\frac{\partial}{\partial\xi}r\tilde{q}_\xi + \frac{1}{\delta}\frac{\partial}{\partial\zeta}\tilde{q}_\zeta = 0, \tag{4.1}$$

$$\underline{2\sin\gamma\tilde{q}_\zeta} - 2\cos\gamma\tilde{q}_\theta = -\underline{\frac{\partial\tilde{p}}{\partial\xi}} + \frac{\partial^2\tilde{q}_\xi}{\partial\zeta^2}, \tag{4.2}$$

$$\underline{-2\cos\gamma\tilde{q}_\zeta} + 2\cos\gamma\tilde{q}_\xi = \frac{\partial^2\tilde{q}_\theta}{\partial\zeta^2}, \tag{4.3}$$

$$0 = -\frac{\partial\tilde{p}}{\partial\zeta}. \tag{4.4}$$

Since the inviscid azimuthal velocities are $\sim \alpha r/2\beta$, it is convenient to introduce:‡

$$\{\tilde{q}_\xi, \tilde{q}_\theta, \tilde{q}_\zeta\} = \frac{\alpha_I(t)}{2\beta}\{r\tilde{F}, r\tilde{\omega}, \tilde{H}\}. \tag{4.5}$$

Equations (4.1) and (4.4) imply that $\tilde{p}$ and $\tilde{q}_\zeta$ are small; therefore, the underlined terms in (4.2)–(4.3) are neglected, and the solution of the remaining balance yields:

$$\tilde{F} + \mathrm{i}\tilde{\omega} = A\,\mathrm{e}^{k\zeta} + B\,\mathrm{e}^{-k\zeta}, \tag{4.6}$$

where

$$k = (\cos\gamma)^{\frac{1}{2}}(1+\mathrm{i}) \quad (\mathrm{i} = \sqrt{-1}).$$

The (complex) $O(1)$ coefficients A and B are in general functions of r and t, determined by boundary conditions and matching requirements.

A useful quantity in the subsequent calculations is the volume transport in the $\hat{\xi}$ direction. In the shear region $0 \leqslant \zeta \leqslant \tilde{S}$ this can be represented by

$$\tilde{\chi} = \int_0^{|\delta\tilde{S}|} \tilde{q}_\xi\,\mathrm{d}(\delta\zeta) = \frac{\alpha_I(t)}{2\beta}r\delta\tilde{Q}, \tag{4.7a}$$

† The typical response time of these regions is $|\epsilon|/\beta$, i.e. about one revolution of the system.

‡ Hopefully, no confusion arises between the velocity component $\tilde{H}$ and the typical height H.

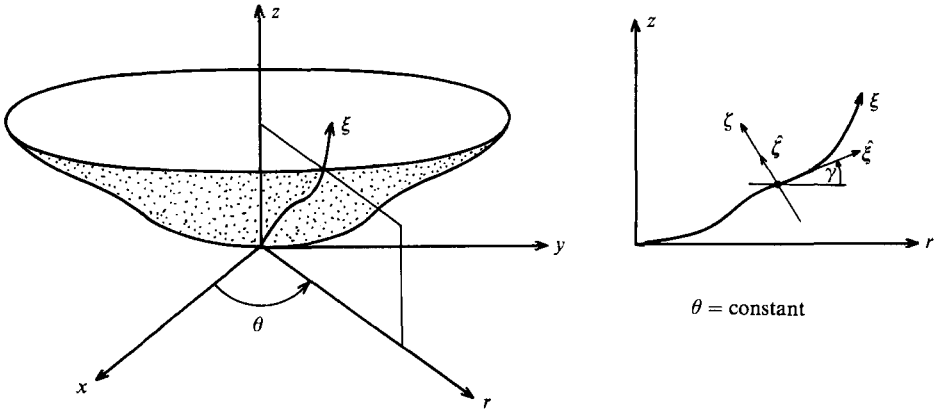

FIGURE 4. The boundary layer coordinates on $z = \sigma(r)$.

where, according to (4.6),

$$\tilde{Q} = \int_0^{|\tilde{S}|} \tilde{F}\,\mathrm{d}\zeta = \mathrm{Re}\left\{\frac{1}{k}[A(\mathrm{e}^{k|\tilde{S}|}-1)-B(\mathrm{e}^{-k|\tilde{S}|}-1)]\right\}. \tag{4.7b}$$

Note that $\tilde{Q}$ and $\tilde{\chi}$ include the sign determined by the main direction of $\tilde{F}$. Integrating (4.1) and using Leibniz's formula yields the normal velocity component at the 'edge' of the shear layer

$$\tilde{H}(\tilde{S}) = -\delta\left[\frac{\tilde{S}}{|\tilde{S}|}\frac{1}{r}\frac{\partial}{\partial\xi}r^2\tilde{Q} - r\tilde{F}\frac{\partial\tilde{S}}{\partial\xi}\right] + \tilde{H}(\zeta = 0). \tag{4.8}$$

The foregoing results are subsequently utilized in the different flow regions, subject to matching and boundary conditions as follows

$$\boldsymbol{q}^{\mathrm{inv}} + \tilde{\boldsymbol{q}} = 0 \text{ on solid walls,} \tag{4.9}$$

$$\tilde{\boldsymbol{q}}\cdot\hat{\boldsymbol{\xi}} + \mathrm{i}\tilde{\boldsymbol{q}}\cdot\hat{\boldsymbol{\theta}} = 0 \quad \text{for } |\tilde{S}| \to \infty \text{ (if applicable).} \tag{4.10}$$

$$\left.\begin{aligned}\left[\boldsymbol{q}^{\mathrm{inv}} + \tilde{\boldsymbol{q}}\right]_+^- &= 0 \qquad (4.11a)\\ \left[(\mu(\alpha))^{\frac{1}{2}}\frac{\partial\tilde{\boldsymbol{q}}}{\partial\zeta}\right]_+^- &= 0 \qquad (4.11b)\end{aligned}\right\} \text{ on interface.}$$

In addition, global volume conservation is required. For the control volume of figure 5, with the aid of (2.11), (4.5), and (4.7), this reads:

$$2\pi r\left\{\left[\int_{z^{\mathrm{B}}}^{z^{\mathrm{T}}}\left[\boldsymbol{q}^{\mathrm{inv}} - |\epsilon|\frac{\Phi(\alpha)}{1+\epsilon\alpha}r\hat{\boldsymbol{r}}\right]\cdot\hat{\boldsymbol{r}}\,\mathrm{d}z + \Sigma\,\tilde{\chi}\right\} = 0, \tag{4.12}$$

where the summation is performed over all the Ekman shear layers cut by the cylinder r = constant. In view of (3.6) and (4.7) the contributions of the 'inviscid' and 'viscous' terms in (4.12) are $O(\epsilon H)$ and $O(E^{\frac{1}{2}}/\beta)$, respectively.† In the case $\lambda = E^{\frac{1}{2}}/|\epsilon|\,\beta H \gg 1$ considered here, the contribution of the first term is small. Thus, to leading order in λ, upon employment of (4.7a), the volume conservation reads

$$\Sigma\,(\delta\tilde{Q}) = 0, \tag{4.13}$$

† See footnote ‡ on p. 35.

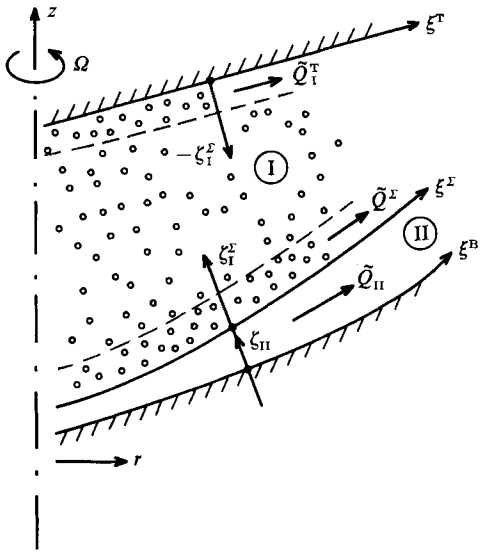

FIGURE 5. Various systems employed in the matching analysis. (Here $s = -1$.)

where, again, summation is performed over all the shear layers cut by r = constant. Recall that $\delta = (\mu(\alpha))^{\frac{1}{2}}E^{\frac{1}{2}}$ with $\alpha = \alpha_{\mathrm{I}}(t)$ in the mixture and $\alpha = 0$ (thus, $\mu(\alpha) = 1$) in the pure fluid.

5. Thin pure fluid layer – the matched flow field

Consider the configuration of figure 5, where the thickness of the pure fluid layer is $O(E^{\frac{1}{2}})$. This situation is typical of the initial stage, at least.

At the collecting top plate $-\zeta$ extends into the mixture core I and $\tilde{S}$ can be regarded as $-\infty$. Applying the conditions (4.9)–(4.10), the coefficients of (4.6) and the corresponding volume transport (4.7*b*) read

$$A_{\mathrm{I}}^{\mathrm{T}} = -\mathrm{i}\omega_{\mathrm{I}}; \quad B_{\mathrm{I}}^{\mathrm{T}} = 0; \quad \tilde{Q}_{\mathrm{I}}^{\mathrm{T}} = -\omega_{\mathrm{i}}/2(\cos\gamma^{\mathrm{T}})^{\frac{1}{2}}. \tag{5.1}$$

Examine next the flow near the bottom. Since the location of the interface differs only by an $O(E^{\frac{1}{2}})$ amount from $z^{\mathrm{B}}(r)$, the pitch angle γ^{Σ} can be approximated by the known value γ^{B}. The shear layer on the interface induces the decaying viscous correction

$$\tilde{F}_{\mathrm{I}} + \mathrm{i}\tilde{\omega}_{\mathrm{I}} = B_{\mathrm{I}}^{\Sigma}\exp(-k^{\mathrm{B}}\zeta_{\mathrm{I}}^{\Sigma})$$

in the mixture region $\zeta_{\mathrm{I}}^{\Sigma} \geqslant 0$. The viscous component in the pure fluid region $0 \leqslant \zeta_{\mathrm{II}} \leqslant \tilde{S}$ is

$$\tilde{F}_{\mathrm{II}} + \mathrm{i}\tilde{\omega}_{\mathrm{II}} = A_{\mathrm{II}}\,\mathrm{e}^{k^{\mathrm{B}}\zeta_{\mathrm{II}}} + B_{\mathrm{II}}\,\mathrm{e}^{-k^{\mathrm{B}}\zeta_{\mathrm{II}}}.$$

Here $k^{\mathrm{B}} = (\cos\gamma^{\mathrm{B}})^{\frac{1}{2}}(1+\mathrm{i})$, and (4.6) and (4.10) are employed. Applying the no-slip conditions (4.9) at $\zeta_{\mathrm{II}} = 0$ and the continuity requirements (4.11) at $\zeta_{\mathrm{I}}^{\Sigma} = 0$ and $\zeta_{\mathrm{II}} = \tilde{S}$ yields, after some arrangement:

$$A_{\mathrm{II}} + B_{\mathrm{II}} + \mathrm{i}\omega_{\mathrm{II}} = 0, \tag{5.2a}$$

$$-B_{\mathrm{I}}^{\Sigma} + A_{\mathrm{II}}\,\mathrm{e}^{k^{\mathrm{B}}\tilde{S}} + B_{\mathrm{II}}\,\mathrm{e}^{-k^{\mathrm{B}}\tilde{S}} - \mathrm{i}(\omega_{\mathrm{I}} - \omega_{\mathrm{II}}) = 0, \tag{5.2b}$$

$$-B_{\mathrm{I}}^{\Sigma} + A_{\mathrm{II}}\,\mathrm{e}^{k^{\mathrm{B}}\tilde{S}} + B_{\mathrm{II}}\,\mathrm{e}^{-k^{\mathrm{B}}\tilde{S}} \tag{5.2c}$$

here $\omega_{\mathrm{I,II}}$ refer to the inviscid component. Also, recall the 'inviscid' relationship (3.7)

$$\omega_{\mathrm{I}} = \omega_{\mathrm{II}} - s. \tag{5.2d}$$

The volume conservation (4.13) upon substituting (5.1) and (5.2*a*, *c*, *d*) gives

$$2\,\mathrm{Re}\{(1-\mathrm{i})A_{\mathrm{II}}\} + (1+R)\omega_{\mathrm{I}} = -s, \tag{5.2e}$$

where

$$R = R(r,t) = \left(\mu(\alpha_{\mathrm{I}}(t))\frac{\cos\gamma^{\mathrm{B}}}{\cos\gamma^{\mathrm{T}}}\right)^{\frac{1}{2}}. \tag{5.3}$$

Thus, the linear system (5.2) practically defines the five velocity field functions ω_{I}, $\omega_{\mathrm{II}}, A_{\mathrm{II}}, B_{\mathrm{II}}, B_{\mathrm{I}}^{\Sigma}$ in terms of the parameter $\tilde{S}$, which represents the at present unknown thickness of the pure fluid layer. More explicit expressions are sought for further investigation of the flow. To this end, after some algebra, a single equation for A_{II} is obtained as follows:

$$A_{\mathrm{II}}[(2+m)\,\mathrm{e}^{2k^{\mathrm{B}}\tilde{S}} - m] + \mathrm{i}\frac{2m}{1+R}\mathrm{Re}\{(1-\mathrm{i})A_{\mathrm{II}}\} = -\mathrm{i}s\left[(1+m)\,\mathrm{e}^{k^{\mathrm{B}}\tilde{S}} - m\frac{R}{1+R}\right], \tag{5.4}$$

where

$$m = (\mu(\alpha_{\mathrm{I}}))^{\frac{1}{2}} - 1.$$

However, simple specific expressions for the coefficients A_{II}, etc. can be obtained for $m = 0$ only (this corresponds to the dilute limit $\alpha_{\mathrm{I}} \to 0$ or to the assumption that the effective viscosities of pure fluid and mixture are equal). Thus, for $\mu(\alpha_{\mathrm{I}}) = 1$, equations (5.4), (5.2) and (4.7*b*) give:

$$\left.\begin{aligned} A_{\mathrm{II}} &= -\tfrac{1}{2}\mathrm{i}s\,\mathrm{e}^{-k^{\mathrm{B}}\tilde{S}}, \\ \omega_{\mathrm{I}} &= \frac{-s}{1+R}[1 - \mathrm{Re}\{(1+\mathrm{i})\,\mathrm{e}^{-k^{\mathrm{B}}\tilde{S}}\}] = \omega_{\mathrm{II}} - s, \\ B_{\mathrm{II}} &= -\mathrm{i}(s+\omega_{\mathrm{I}}) + \tfrac{1}{2}\mathrm{i}s\,\mathrm{e}^{-k^{\mathrm{B}}\tilde{S}}. \end{aligned}\right\} \tag{5.5}$$

Further substitution into (4.7*b*) yields the following important result: $-s\tilde{Q}_{\mathrm{II}}$ reaches its absolute maximum as $\tilde{S}_{\mathrm{crit}} = \pi/(\cos\gamma^{\mathrm{B}})^{\frac{1}{2}}$, where

$$(-s\tilde{Q}_{\mathrm{II}})_{\max} = \frac{1}{(\cos\gamma^{\mathrm{B}})^{\frac{1}{2}}}\frac{1}{2}\left[\frac{1}{2} + \frac{R}{1+R} + \mathrm{e}^{-\pi}\frac{1-R}{1+R}\right](1+\mathrm{e}^{-\pi}), \tag{5.6}$$

(cf. figure 6).† This value differs only slightly, by the $\mathrm{e}^{-\pi}$ terms, from the asymptotic $\tilde{S} \to \infty$ limit. A similar behaviour of $\tilde{Q}_{\mathrm{II}}$ has been found for the more realistic case $\mu(\alpha_{\mathrm{I}}) > 1$; $\tilde{S}_{\mathrm{crit}}$ is unchanged but $|Q_{\mathrm{II}}|_{\max}$ is somewhat larger than the value of (5.6).

In the foregoing analysis the variable $\tilde{S}$, which measures the local instantaneous thickness of the pure fluid layer on the coordinate ζ, enters the solution as a parameter. In the actual flow field $\tilde{S} = \tilde{S}(\xi, t)$ is defined by the motion of the interface, equation (2.16). In the boundary-layer coordinates of the bottom plate the interface is expressed as

$$\Sigma(\boldsymbol{r}, t) = \zeta_{\mathrm{II}} - \tilde{S}(\xi, t) = 0, \tag{5.7}$$

and the appropriate equations of motion, in account of (4.5), reads

$$\frac{\partial\tilde{S}}{\partial t} + \left(\frac{\alpha_{\mathrm{I}}}{2\beta}r\tilde{F} + s\frac{\Phi(\alpha_{\mathrm{I}})}{\alpha_{\mathrm{I}}}r\hat{\boldsymbol{r}}\cdot\hat{\boldsymbol{\xi}}\right)\frac{\partial\tilde{S}}{\partial\xi} - \left(\frac{\alpha_{\mathrm{I}}}{2\beta}\tilde{H} + s\frac{\Phi(\alpha_{\mathrm{I}})}{\alpha_{\mathrm{I}}}r\hat{\boldsymbol{r}}\cdot\hat{\boldsymbol{\zeta}}\right)\frac{1}{\delta_{\mathrm{II}}} = 0. \tag{5.8}$$

Here, of course, $\tilde{F}$ and $\tilde{H}$ are evaluated at $\zeta_{\mathrm{II}} = \tilde{S}$.

† For parallel plates $R = 1$ in which case (5.6) is consistent with (3.1*c*) of Amberg *et al.* (1986).

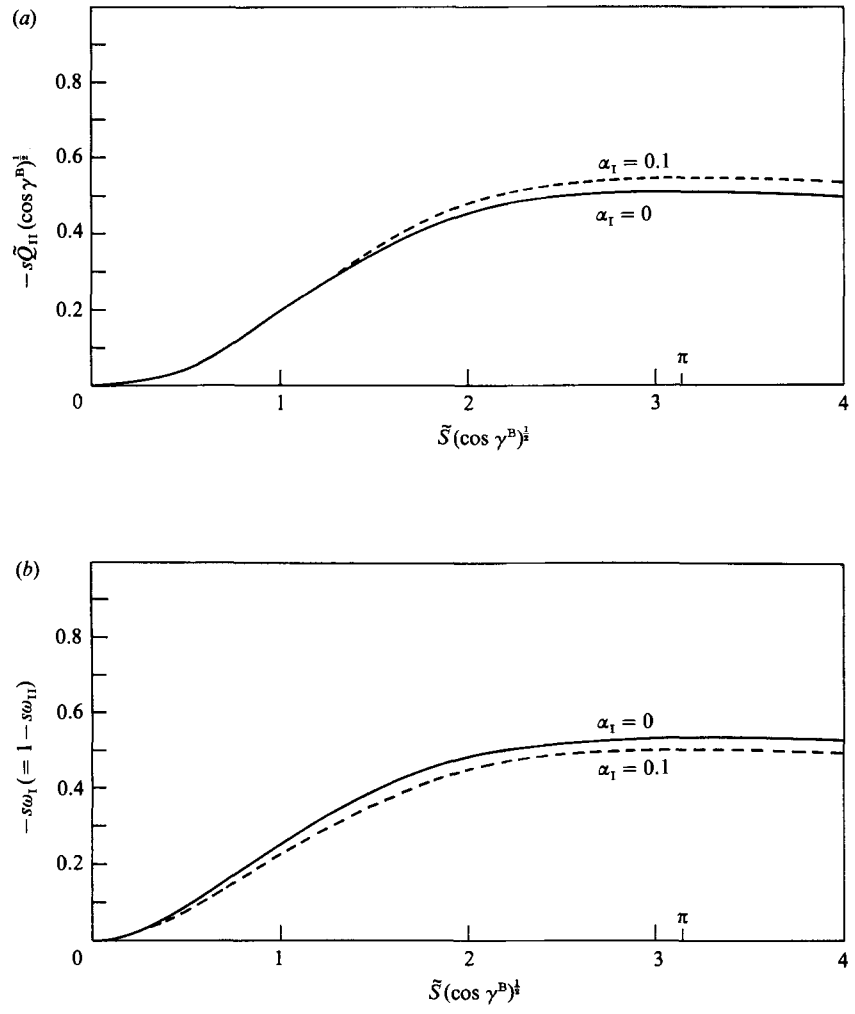

FIGURE 6. Volume flux and inviscid angular velocity *vs.* local thickness of the pure fluid layer for $\cos\gamma^B/\cos\gamma^T = \frac{1}{2}\sqrt{3}$.

Substituting (4.8) (with boundary condition zero on the plate) into (5.8) and expressing the dot products in terms of γ^B yields

$$E^{\frac{1}{2}}\frac{\partial\tilde{S}}{\partial t}+\left(\frac{E^{\frac{1}{2}}\alpha_I}{2\beta}\right)\frac{1}{r}\frac{\partial}{\partial\xi}r^2\tilde{Q}+sE^{\frac{1}{2}}\frac{\Phi(\alpha_I)}{\alpha_I}r\cos\gamma^B\frac{\partial\tilde{S}}{\partial\xi}=-s\sin\gamma^B\frac{\Phi(\alpha_I)}{\alpha_I}r. \tag{5.9}$$

This equation expresses the critical features of the thin pure fluid layer at the bottom plate. The right-hand side $O(1)$ term reproduces the tendency of the dispersed buoyant particles to depart from the plate. (Recall that a consistent definition requires $\gamma^B > 0$ for light particles $s < 0$ and vice versa, therefore this term is always positive.) The only term of comparable order of magnitude on the left-hand side is the second one, provided that $(E^{\frac{1}{2}}\alpha_I\cos\gamma^B/2\beta) = O(\sin\gamma^B)$; this term represents the 'suction' of the Ekman layers. The last expression on the left-hand side is always negligible. The first term of (5.9) indicates that $\tilde{S}$ varies on the time

scale $E^{\frac{1}{2}}$, which is very short compared to the separation interval.† Consequently, if the pure fluid layer remains thin it is quasi-steady and satisfies the balance:

$$\left(\frac{E^{\frac{1}{2}}\alpha_1}{2\beta}\right)\cos\gamma^{\mathrm{B}}\frac{\mathrm{d}}{\mathrm{d}r}r^2\tilde{Q}_{\mathrm{II}} = |\sin\gamma^{\mathrm{B}}|\frac{\Phi(\alpha_1)}{\alpha_1}r^2. \tag{5.10}$$

However, under circumstances to be clarified below, the Ekman layer suction may be too weak to satisfy the requirement (5.10). In this case the term $E^{\frac{1}{2}}(\partial\tilde{S}/\partial t)$ takes over in (5.9), which implies a quickly thickening layer.

Let r_1 be the starting position ($\tilde{S}=0, \tilde{Q}_{\mathrm{II}}=0$) of the thin layer, which corresponds to r_{i} for light particles and to 1 for heavy ones, cf. figure 2. Integrating (5.10) between r_1 and r gives

$$\tilde{Q}_{\mathrm{II}}|_r = \left(\frac{2\beta}{\alpha_{\mathrm{I}}E^{\frac{1}{2}}}\right)\frac{\Phi(\alpha_{\mathrm{I}})}{\alpha_{\mathrm{I}}}\frac{1}{r^2}\int_{r_1}^{r}|\tan\gamma^{\mathrm{B}}(\bar{r})|\,\bar{r}^2\,\mathrm{d}\bar{r}, \tag{5.11}$$

which implicitly defines $\tilde{S}(r,t)$ via the relationships for $\alpha_{\mathrm{I}}(t)$ and $\tilde{Q}_{\mathrm{II}}(\tilde{S})$ obtained previously.

First, consider the implications of (5.11) for the light particle mixture. Typically, $\tilde{S}$ (and $\tilde{Q}_{\mathrm{II}}$) increase with $r\,(>\mathrm{r_i})$ until some r_{crit} where $\tilde{Q}_{\mathrm{II}}$ reaches its maximum and $\tilde{S}_{\mathrm{crit}} = \pi/(\cos\gamma^{\mathrm{B}}(r_{\mathrm{crit}}))^{\frac{1}{2}}$. Beyond this r_{crit} the balance (5.11) can no longer be satisfied, i.e. the pure fluid layer will not remain thin.

Secondly, observe that for heavy particles mixtures Q_{II} is negative, i.e. the flux is towards the centre. Equation (5.11) indicates that $\tilde{S}$ increases as r (and $\tilde{Q}_{\mathrm{II}}$) decreases, until, again, some r_{crit} where $\tilde{Q}_{\mathrm{II}}$ is minimal. For $r < r_{\mathrm{crit}}$, equation (5.11) has no solution which, again, attests the lack of a thin pure fluid layer in this domain.

Since $|\tilde{Q}_{\mathrm{II}}|_{\max}$ is of order unity it follows that $|r_1 - r_{\mathrm{crit}}| \sim O((E^{\frac{1}{2}}\alpha_{\mathrm{I}}/\beta)\cot\gamma^{\mathrm{B}})$. This conclusion is worth emphasizing: the radial extent of the pure fluid thin layer is restricted to $O(E^{\frac{1}{2}}\alpha_{\mathrm{I}}\cot\gamma^{\mathrm{B}}/\beta)$ due to the limited capability of the Ekman layers to transport the fluid sucked into this region. This limitation has no counterpart in the gravitational settling. In this respect it is instructive to consider an alternative purely kinematic derivation of (5.11) as follows. The pure fluid volume balance for the region bounded by r, r_1, the steady interface and the bottom plate is:

$$2\pi\frac{\alpha_{\mathrm{I}}E^{\frac{1}{2}}}{2\beta}r^2\tilde{Q}_{\mathrm{II}}|_{\mathrm{r}} = -2\pi\int_r^{r_1}\boldsymbol{j}_{\mathrm{C}}\cdot\hat{\boldsymbol{n}}\frac{r\,\mathrm{d}r}{\cos\gamma^{\mathrm{B}}}, \tag{5.12}$$

where (4.7) has been employed and $\boldsymbol{j}_{\mathrm{C}}$ is taken at the interface. Using the kinematic relationship (A 11), equations (2.8), (2.10) and accounting for the condition $\boldsymbol{j}_{\mathrm{D}}\cdot\hat{\boldsymbol{n}} = 0$ it follows that at the interface:

$$\boldsymbol{j}_{\mathrm{C}}\cdot\hat{\boldsymbol{n}} = -s\frac{\Phi(\alpha_{\mathrm{I}})}{\alpha_{\mathrm{I}}}r\hat{\boldsymbol{r}}\cdot\hat{\boldsymbol{n}} = -\frac{\Phi(\alpha_{\mathrm{I}})}{\alpha_{\mathrm{I}}}r|\sin\gamma^{\mathrm{B}}|.$$

Substituting into (5.12) and rearranging yields, again, (5.11). It is now more evident that the last term of (5.11) represents the rate of suction into the pure fluid layer, which can be balanced as long as the Ekman layers are able to carry it away in the radial direction.

† Nevertheless, the Ekman balances are quasi-steady because (5.9) is of interest for $(E^{\frac{1}{2}}/\beta) \geqslant 1$, which implies $E^{\frac{1}{2}} \gg |\epsilon|\beta$. See footnote † on p. 35.

Since r_i and the representative value of $(E^{\frac{1}{2}}\alpha_1 \cot\gamma^B/\beta)$ can both vary in a large range for miscellaneous systems, it is convenient to distinguish between two typical cases:

(i) $|r_{crit}-r_1| \geqslant 1-r_i$, i.e. the pure fluid layer between the bottom wall and mixture is thin everywhere. The solution of the present section covers the entire flow of interest. The shape of the interface apparently resembles that of the gravitational settling.

(ii) $|r_{crit}-r_1| < 1-r_i$. The present quasi-steady thin, viscous, pure fluid layer expands into the 'thick' bulk considered in the next section.

For both cases, however, it should be born in mind that $|r_{crit}-r_1|$ provides the locus beyond which a thin pure fluid layer cannot prevail. The actual detachment position of the interface is either at $r_d(t)$ or at the 'vertical' front $r_F(t)$, according to the shortest distance from r_1, cf. §7.

6. Thick pure fluid layer – the matched flow field

Beyond r_{crit} obtained in the previous section, the flow field can be represented by two inviscid bulks I and II, each of them bounded by distinct Ekman layers, see figure 7. This case was analysed by Greenspan & Ungarish (1985*b*). Some relevant results are rederived here (in a slightly different approach) for the sake of completeness.

The tangential flow 'corrections' in shear layers are given by (4.5)–(4.6). Superposition on the inviscid components (3.6)–(3.7) and employment of (4.9)–(4.11) (note that $|\tilde{S}|\to\infty$ for all the concerned shear regions) give the coefficients A, B of (4.6) for every layer in terms of ω_I or ω_{II}; $\tilde{Q}$ is subsequently obtained via (4.7*b*). The results are summarized in table 1, where $\mu^{\frac{1}{2}} = (\mu(\alpha_I))^{\frac{1}{2}}$ and $\gamma = \gamma(r)$ is the local inclination of the appropriate surface, measured counterclockwise from the plane z = constant. Note that at the interface $\tilde{F}^{\Sigma}_{II} = \tilde{F}^{\Sigma}_{I} = 0$. Substituting the foregoing results into the volume conservation requirement (4.13) on account of (3.7*b*) results:

$$\omega_I = -\frac{s}{1+R}, \quad \omega_{II} = s+\omega_I, \tag{6.1}$$

where, again

$$R = \left(\mu(\alpha_I)\frac{\cos\gamma^B}{\cos\gamma^T}\right)^{\frac{1}{2}}.$$

Let the interface be:

$$\Sigma(\boldsymbol{r},t) = z - S(r,t) = 0, \tag{6.2}$$

with $\boldsymbol{n} = \nabla\Sigma = \hat{\boldsymbol{z}} - (\partial S/\partial r)\,\hat{\boldsymbol{r}}$ and, obviously, $\cos\gamma^{\Sigma} = [1+(\partial S/\partial r)^2]^{-\frac{1}{2}}$. To determine its motion by (2.16) the value of $\boldsymbol{q}\cdot\hat{\boldsymbol{n}}$ on Σ is required. To this end consider the volume balance in the control volume of figure 8

$$(\boldsymbol{q}_{II}\cdot\hat{\boldsymbol{n}})_{\Sigma}\left(\frac{r\,dr}{\cos\gamma^{\Sigma}}\right)+\left[r\tilde{\chi}^{\Sigma}_{II}+r\tilde{\chi}^{B}_{II}+r\int_{z^B}^{S}u^{inv}_{II}\,dz\right]_{r}^{r+dr}=0, \tag{6.3}$$

which, on account of (4.7), table 1, (3.6) and (6.1) yields

$$(q_{II}\cdot\hat{\boldsymbol{n}})_{\Sigma} = s\frac{E^{\frac{1}{2}}\alpha_I}{4\beta}\mu^{\frac{1}{2}}\cos\gamma^{\Sigma}\frac{1}{r}\frac{\partial}{\partial r}r^2\left[\frac{1}{(\cos\gamma^T)^{\frac{1}{2}}+(\mu\cos\gamma^B)^{\frac{1}{2}}}+\frac{1}{(\cos\gamma^{\Sigma})^{\frac{1}{2}}}\frac{1}{1+\mu^{\frac{1}{2}}}\right]. \tag{6.4}$$

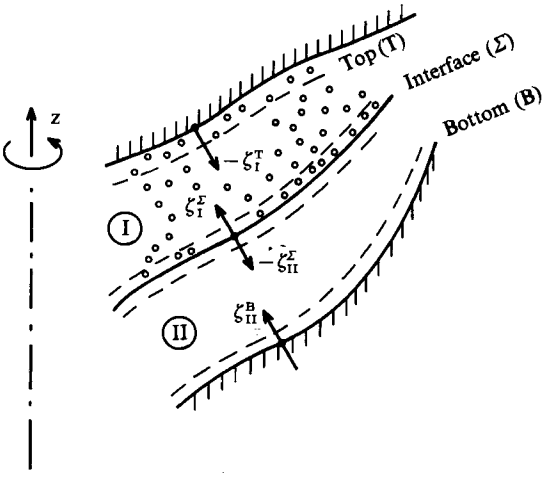

FIGURE 7. Typical configuration of thick pure fluid layer (bulk), $s = -1$.

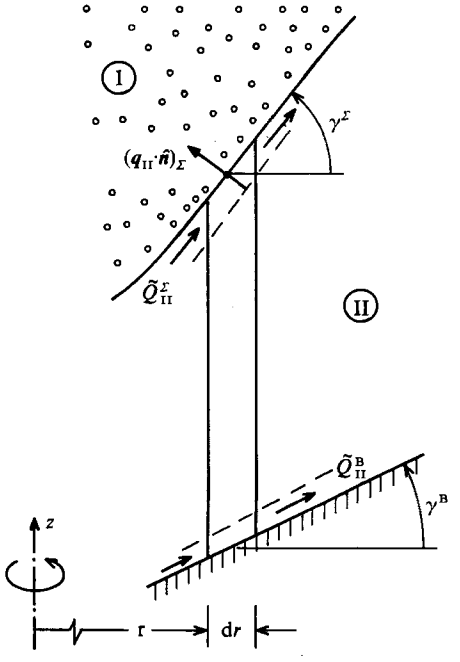

FIGURE 8. Control volume for calculating the normal velocity of interface, $s = -1$.

Since on the interface $\boldsymbol{q}_{\mathrm{II}} = \boldsymbol{q}_{\mathrm{I}}$ and $\hat{\boldsymbol{n}} = (\nabla\Sigma)\cos\gamma^{\Sigma}$, the substitution of (6.4) into (2.16) gives:

$$\frac{\partial S}{\partial t} - s\frac{E^{\frac{1}{2}}\alpha_{\mathrm{I}}}{4\beta}\mu^{\frac{1}{2}}\frac{1}{r}\frac{\partial}{\partial r}r^2\left(\frac{1}{(\cos\gamma^{\mathrm{T}})^{\frac{1}{2}}+(\mu\cos\gamma^{\mathrm{B}})^{\frac{1}{2}}}+\frac{1}{(\cos\gamma^{\Sigma})^{\frac{1}{2}}}\frac{1}{1+\mu^{\frac{1}{2}}}\right)+s\frac{\Phi(\alpha_{\mathrm{I}})}{\alpha_{\mathrm{I}}}r\frac{\partial S}{\partial r}=0, \tag{6.5}$$

subject to the initial condition $S(r,0) = z^{\mathrm{B}}(r)$. Actually, when $S - z^{\mathrm{B}} = O(E^{\frac{1}{2}})$ an

Location of layer	Notation	$\delta/E^{\frac{1}{3}}$	A	B	$2(\cos\gamma)^{\frac{1}{2}}\tilde{Q}$
Top of container	$A_{\mathrm{I}}^{\mathrm{T}}$, etc.	$\mu^{\frac{1}{2}}$	$-\mathrm{i}\omega_{\mathrm{I}}$	0	$-\omega_{\mathrm{I}}$
Above interface	A_{I}^{Σ}, etc.	$\mu^{\frac{1}{2}}$	0	$\dfrac{\mathrm{i}s}{1+\mu^{\frac{1}{2}}}$	$\dfrac{s}{1+\mu^{\frac{1}{2}}}$
Below interface	A_{II}^{Σ}, etc.	1	$-\mathrm{i}\dfrac{s\mu^{\frac{1}{2}}}{1+\mu^{\frac{1}{2}}}$	0	$-\dfrac{s\mu^{\frac{1}{2}}}{1+\mu^{\frac{1}{2}}}$
Bottom of container	$A_{\mathrm{II}}^{\mathrm{B}}$, etc.	1	0	$-\mathrm{i}\omega_{\mathrm{II}}$	$-\omega_{\mathrm{II}}$

TABLE 1

equation similar to (5.9) should be used as an 'inner' asymptotic limit of (6.5). The difference, however, is insignificant on the $O(1)$ timescale. A similar argument justifies the incompatibility of $\omega_{\mathrm{I,II}}$ with initial conditions.

7. The steep parts of the interface

Heuristic considerations indicate that when $(E^{\frac{1}{3}}\alpha_{\mathrm{I}}/\beta)$ is not small the detached part of the interface should be (at least piecewise) abruptly inclined with respect to the centrifugal field. It is therefore suggested to treat the interface as a 'vertical' cylinder $r = r_{\mathrm{v}}(t)$ at the front $r = r_{\mathrm{F}}(t)$ and at detachment radius $r_{\mathrm{d}}(t)$ (provided that $r_{\mathrm{i}} < r_{\mathrm{crit}} < 1$). In this case, the volume flux adjustments required by the $E^{\frac{1}{2}}$ layers at these positions are performed via $E^{\frac{1}{3}}$ 'vertical' shear layers, where the order of magnitude of the velocity correction is

$$\{\hat{u}, \hat{v}, \hat{w}\} = O\left\{E^{\frac{1}{2}}\frac{\alpha}{\beta}, E^{\frac{1}{3}}\frac{\alpha}{\beta}, E^{\frac{1}{6}}\frac{\alpha}{\beta}\right\}.$$

The radial velocity of 'vertical' interface, u_{v}, is obtained as follows. The volume balance of mixture at $r = r_{\mathrm{v}}$ is (cf. figure 9)

$$(z^{\mathrm{T}} - z^{\Sigma})\boldsymbol{j}\cdot\hat{\boldsymbol{r}} = \tilde{\chi}_{\mathrm{I}}^{\mathrm{T}} + \tilde{\chi}_{\mathrm{I}}^{\Sigma} = \frac{\alpha_{\mathrm{I}}E^{\frac{1}{2}}}{2\beta} r_{\mathrm{v}}(\tilde{Q}_{\mathrm{I}}^{\mathrm{T}} + \tilde{Q}_{\mathrm{I}}^{\Sigma}). \tag{7.1}$$

Using this equation, the kinematic relationships (A 5) and (A 9), equations (2.15) and (2.8) one gets:

$$u_{\mathrm{v}} = s\frac{(1-\alpha)^2}{\mu(\alpha)} r_{\mathrm{v}} + \frac{E^{\frac{1}{2}}\alpha_{\mathrm{I}}}{2\beta}\frac{1}{(z^{\mathrm{T}} - z^{\Sigma})}(\tilde{Q}_{\mathrm{I}}^{\mathrm{T}} + \tilde{Q}_{\mathrm{I}}^{\Sigma}). \tag{7.2}$$

Time integration of this equation produces the loci $r_{\mathrm{F}}(t)$ and $r_{\mathrm{d}}(t)$ subject to the initial conditions $r_{\mathrm{F}}(0) = r_{\mathrm{i}}$ (r_{i} for $s = 1$ and 1 for $s = -1$) and $r_{\mathrm{d}}(0) = r_{\mathrm{crit}}(0)$. Approximations to these variables are $r_{\mathrm{F}}(t)$ of the PNK theory (Appendix B) and $r_{\mathrm{crit}}(t)$.

The first term on the left-hand side of (7.2) represents the contribution of the basic separation velocity, while the enhancement (second) one becomes significant when $E^{\frac{1}{2}}\alpha/2\beta$ is $O(1)$. It is emphasized that the Coriolis acceleration required for this additional radial component is supplied by the viscous shear in the $E^{\frac{1}{3}}$ layer; in the inviscid cores outside this layer the radial velocity is negligibly small. This is untypical of the gravitational parallel enhancement effect.

There is an apparent similarity between the flow in the present $E^{\frac{1}{3}}$ shear layer and that adjacent to the fluid front in the (linear) filling of a rotating cylinder studied by

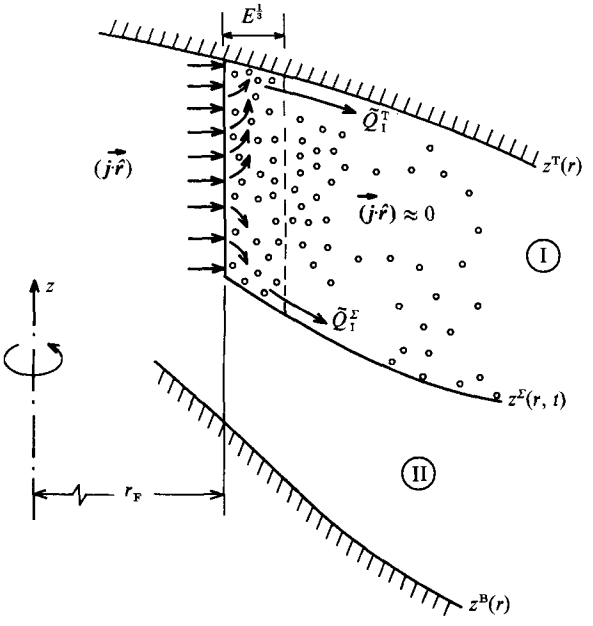

FIGURE 9. Schematic volume flow in mixture region at perpendicular front $r_F(t)$, $s = 1$.

Ungarish & Greenspan (1984*a*). In addition, the azimuthal velocity discontinuities at r_F and r_d can be smoothed via $E^{\frac{1}{4}}$ shear layers. The arrangement of the Ekman layers resembles the problem analysed by Moore & Saffman (1969), where a strong recirculation in the 'vertical' layers has been predicted. The flow details in these regions are not pursued in the present work.

8. Example

It is convenient to illustrate several interesting results and implications of the present study via the following particular simple examples.

Consider the containers of figure 2: the top is flat, $z^T = \text{constant}$, $\gamma^T = 0$; the bottom is a cone, $z^B = -s \tan|\gamma^B| r$, $\gamma^B = \text{constant} = 30°$ and there is no inner boundary, $r_i = 0$. Let $\alpha_M = 1$ and recall that $s = 1$ or -1 for heavy or light particles mixtures, respectively.

For the sector where the pure fluid layer is thin (5.11) yields

$$r - \frac{r_I^3}{r^2} = 3\frac{E^{\frac{1}{2}}\alpha_I(t)}{2\beta}\frac{\alpha_I}{\Phi(\alpha_I)}\cot|\gamma^B|\,\tilde{Q}_{II}(\tilde{S}). \tag{8.1}$$

Using the appropriate $\tilde{Q}_{II}(\tilde{S})$ obtained from (5.2), cf. figure 6, $\tilde{S}(r)$ is readily obtained (figure 10). This determines the dependence of the flow variables on r, because these were already defined as functions of $\tilde{S}$, e.g. figure 6(*b*). The position r_{crit} is clearly shown in figure 10. For small α_I and neglecting $O(e^{-\pi})$ terms in (5.6) one gets

$$r_{crit}\left[1-\left(\frac{r_I}{r_{crit}}\right)^3\right] \approx -s\frac{3}{4}\frac{E^{\frac{1}{2}}\alpha_I}{2\beta}\frac{(\cos\gamma^B)^{\frac{1}{2}}}{\sin|\gamma^B|}\left(1+\frac{2(\cos\gamma^B)^{\frac{1}{2}}}{1+(\cos\gamma^B)^{\frac{1}{2}}}\right) = -2.74\,s\frac{E^{\frac{1}{2}}\alpha_I}{2\beta}, \tag{8.2}$$

which underestimates the exact value of $|r_{crit} - r_I|$.

Figure 10 also emphasizes the sensitivity of the pure fluid layer structure to the

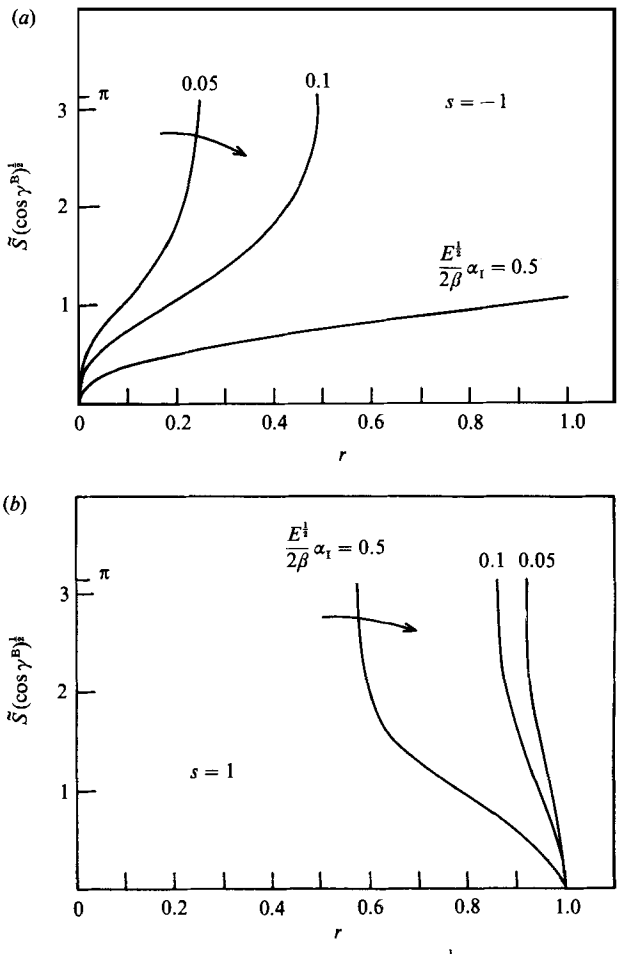

FIGURE 10. Pure fluid layer thickness *vs.* r for various $(E^{\frac{1}{2}}/2\beta)\alpha_I$ and $\alpha_I = 0.1$ in conical container $\gamma^B = -s\cdot 30°, \gamma^T = 0, r_i = 0$. (*a*) Light particles, $s = -1$; (*b*) heavy particles, $s = 1$. The arrow indicates direction of change with time. r_{crit} corresponds to $\tilde{S}(\cos\gamma^B)^{\frac{1}{2}} = \pi$.

value of $(E^{\frac{1}{2}}/\beta)\alpha_I$. Since $\alpha_I \approx \alpha(0)\,e^{-2st}$, the change of the quasi-steady $\tilde{S}(r)$ with time is qualitatively indicated by the arrow in these figures.

For the sector where the pure fluid layer is thick, $r \in \text{int}\,(r_{crit}, r_F)$, (6.1) gives:

$$\omega_I = -\frac{s}{1+0.931(\mu(\alpha_I))^{\frac{1}{2}}}, \quad \omega_{II} = \frac{s(0.931(\mu(\alpha_I))^{\frac{1}{2}})}{1+0.931(\mu(\alpha_I))^{\frac{1}{2}}}. \tag{8.3}$$

It is anticipated that the interface in this region is of conical shape

$$S(r,t) = a(t) + b(t)\,r, \tag{8.4}$$

with $a(0) = 0$ and $b(0) = \tan\gamma^B$. Hence, $\cos\gamma^\Sigma = (1+b^2(t))^{-\frac{1}{2}}$ and substituting in (6.5) with the aid of (2.12) yields, after some algebra

$$b(t) = b(0)\left(\frac{\alpha_I(t)}{\alpha_I(0)}\right)^{\frac{1}{2}}, \tag{8.5}$$

$$\frac{da}{d\alpha_I} = -\frac{E^{\frac{1}{2}}}{4\beta}\frac{\alpha_I}{\Phi(\alpha_I)}(\mu(\alpha_I))^{\frac{1}{2}}\left[\frac{1}{1+(\cos\gamma^B)^{\frac{1}{2}}} + \frac{1}{1+(\mu(\alpha_I))^{\frac{1}{2}}}\left(1+b^2(0)\frac{\alpha_I}{\alpha_I(0)}\right)^{\frac{1}{4}}\right]. \tag{8.6}$$

t	α	a	arctan (b)	r_{crit}	r_2	$(r_F)_{PNK}$
			$s=-1$			
0.0	0.10	0	30°.0°	0.25	0	1.00
0.5	0.17	−0.039	36.9°	0.64	0.23	0.56
1.0	0.24	−0.103	41.9°	1.40	0.32	0.44
Note: $a(t)+b(t)\,r_2=b(0)$.						
			$s=1$			
0.0	0.10	0	−30°.0°	0.92		0
0.5	0.05	0.020	−22.0°	0.97		0.79
1.0	0.02	0.029	−14.9°	0.99		1.26

TABLE 2

The analytical solution of (8.5) can be readily obtained only in the limit $\alpha_I \ll 1$ (thus, $\mu(\alpha_I)=1$ $\Phi(\alpha)\approx\alpha$) and reads:

$$a(t)=\frac{E^{\frac{1}{2}}\alpha_I(0)}{4\beta}\left[\frac{1}{1+(\cos\gamma^B)^{\frac{1}{2}}}\left(1-\frac{\alpha_I(t)}{\alpha_I(0)}\right)+\frac{2}{5b^2(0)}(1+b^2(0))^{\frac{5}{4}}-\left(1+b^2(0)\frac{\alpha_I(t)}{\alpha_I(0)}\right)^{\frac{5}{4}}\right]. \tag{8.7}$$

For small angles of inclination, $b^2(0)\ll 1$, this can be further estimated by

$$a(t)\approx\frac{E^{\frac{1}{2}}\alpha_I(0)}{4\beta}\left(1-\frac{\alpha_I(t)}{\alpha_I(0)}\right)\left[\frac{1}{1+(\cos\gamma^B)^{\frac{1}{2}}}+\frac{1}{2}\right]. \tag{8.8}$$

The approximation $\alpha_I(t)/\alpha(0)\approx\exp(-2st)$ gives additional insight. Thus, according to (8.4)–(8.8), the Ekman suction represented by $(E^{\frac{1}{2}}\alpha_I/\beta)$ affects the position of the conical interface, but not its inclination b.

The PNK approximation, Appendix B, yields

$$(r_F)_{PNK}=\left\{\frac{1}{2}\left[\frac{\alpha(0)}{\alpha(t)}-1\right]\right\}^{\frac{1}{3}} \quad \text{for } s=1,$$

$$(r_F)^2_{PNK}[3-2(r_F)_{PNK}]=\frac{\alpha(0)}{\alpha(t)} \quad \text{for } s=-1.$$

Some results for $\alpha(0)=0.1, E^{\frac{1}{2}}/\beta=1$, are presented in table 2.

Thus, in the $s=-1$ case the thin pure fluid layer configuration (§5) dominates the flow for $t>0.5$, while in the $s=1$ case r_{crit}, is close to the wall and the flow field displays the bulk structure discussed in §6.

9. Concluding remarks

The flow field of a separating mixture in a rotating axisymmetric container with inclined walls has been analysed. In particular, the development and behaviour of the pure fluid layer adjacent to the inclined boundary from which particles are removed by the centrifugal buoyancy has been elucidated. It is concluded that this flow is governed by $\Xi=E^{\frac{1}{2}}\alpha_I|\cot\gamma^B|/\beta$, which turns out to represent the ratio between the Ekman layer suction and separation velocities.

When Ξ is small the pure fluid layer thickens quickly to form an inviscid core surrounded by thin Ekman layers. The interface between the mixture and pure fluid cores is not perpendicular to the force field. This configuration, as investigated by Greenspan & Ungarish (1985*a*, *b*), is strikingly different from the gravitational settling in tilted containers investigated by Acrivos & Herbolzheimer (1979) and Schneider (1982).

However, for large values of Ξ the inclined pure fluid layer is quasi-steady and its width does not exceed the Ekman thickness $\pi(\mu_c^*/\rho_c^* \Omega^* \cos\gamma^B)^{\frac{1}{2}}$. The Coriolis forces are counteracted by viscous shear. The remaining part of the interface is feasibly perpendicular to the centrifugal field and its radial motion may be augmented via the viscous effects in the accompanying $E^{\frac{1}{3}}$ and $E^{\frac{1}{4}}$ layers. Since this configuration displays resemblance to the gravitational one, an appropriate analog of the PNK theory can be employed.

When $\Xi \sim 1$ the locus $r_d \approx r_{crit}$ roughly demarcates the merging of the thin viscous layer and the thick core of pure fluid, which coexist in the same container, cf. figure 2. The intermediate region has not been considered in detail and is an interesting topic for further investigation.

In any case, the mixture core I and the pure fluid region II rotate in opposite senses. This $O(\epsilon\alpha_I \Omega^*)$ difference in angular velocity measured in the rotating system, is roughly equipartitioned between I and II when the pure fluid layer's thickness is close to or beyond $\pi(\mu_c^*/\rho_c^* \Omega^* \cos\gamma^B)^{\frac{1}{2}}$. If the thickness is smaller, the rotation of the mixture core relative to the container diminishes accordingly.

In the limit $\Xi \to \infty$, which corresponds to non-inclined bottom plate, no pure fluid layer develops, which violates the assumption of the present study. This configuration is essentially similar to the finite cylinder investigated by Ungarish (1986, 1988). Accordingly, for the large values of $\lambda (= E^{\frac{1}{3}}/|\epsilon|\beta H)$ considered here, the angular velocity is very small – in contradiction to the above-mentioned significant rotation which shows up when a pure fluid region exists. This makes a major difference between these two configurations and it can be argued that the critical angle of inclination, γ^B, is $O(E^{\frac{1}{2}})$.

The present results are relevant to the enhancement of separation in large vessels. In this respect it is important to keep in mind the following basic difference between typical gravitational and centrifugal processes. The former is accompanied by a disengagement between the phases remarkably represented by the growth of the pure fluid volume and shrink of the mixture region. The latter type contains, in addition, the less observable but very important effect of squeezing: the local α monotonically varies in time in the mixture region at a rate essentially unaffected by the geometry of the boundaries. Consequently, the motion of the interface, which is a direct indicator of the settling performance in gravity field, may be much less pertinent in the centrifugal case. On the other hand, in the narrowly-spaced disk centrifuge considered by Amberg *et al.* (1986), the process is performed on small timescales during which α is practically constant.

The corresponding flow fields, in meridionally sectioned tanks with inclined wall, display many different features, see Amberg & Greenspan (1987), where additional important references are given.

Other interesting effects may show up for larger values of β when the Coriolis forces on the particle induce an azimuthal component of relative velocity. This case has been treated in configurations where the Ekman layers are probably unimportant. Greenspan (1983), Ungarish & Greenspan (1984*b*) and Schaflinger *et al.* (1986). However, no theory is presently available for the two-phase flow in the Ekman layers

which are thinner than the dispersed particle size, as implied by $\beta \gtrsim 1$. Therefore, the present investigation cannot be straightforwardly extended into that range.

The foregoing results are based on a perturbation involving small $\beta, \epsilon, E^{\frac{1}{2}}$, moderate α and angles of inclination and aspect ratio $O(1)$. A more rigorous expansion (e.g. introducing parameters like $\beta = bE^{\frac{1}{2}}, \epsilon = cE^{\frac{1}{2}}$, etc., as suggested by Greenspan & Ungarish 1985*b*) may indicate validity restrictions of the present approach and the occurrence of additional effects. Moreover, the postulated form of the mixture viscous stress, of the relative velocity and of the mixture boundary conditions are partially debatable. These topics require a great deal of additional study, comparison to numerical computations and, above all, experimental verification. In this respect it is worth emphasizing that several results of this work (e.g. the shape of the interface for different values of Ξ) can be checked by feasible demonstrative experiments of the type performed by Amberg & Greenspan (1987) and Greenspan (private communication). These experiments indeed corroborated the theoretical predictions concerning the absence and occurrence of the thin pure fluid layer for small and large Ξ, respectively. Quantitative measurements of the leading variables $\tilde{S}$ and ω_{I}, which require more sophisticated equipment, will provide the additional necessary information for a critical comparison to the theoretical results obtained here.

The author is grateful to Professor H. P. Greenspan for useful remarks and criticism and for experimental corroboration. This research was partially supported by the National Science Foundation, Grant Number 8519764-DMS.

Appendix A

Some useful kinematic relations between velocities and volume fluxes are summarized below:

$$\boldsymbol{q}_{\mathrm{R}} = \boldsymbol{q}_{\mathrm{D}} - \boldsymbol{q}_{\mathrm{C}}, \tag{A 1}$$

$$(1+\epsilon\alpha)\,\boldsymbol{q} = (1-\alpha)\,\boldsymbol{q}_{\mathrm{C}} + \alpha(1+\epsilon)\,\boldsymbol{q}_{\mathrm{D}}, \tag{A 2}$$

$$\boldsymbol{q}_{\mathrm{D}} = \boldsymbol{q} + \frac{1-\alpha}{1+\epsilon\alpha}\boldsymbol{q}_{\mathrm{R}}, \tag{A 3}$$

$$\boldsymbol{q}_{\mathrm{C}} = \boldsymbol{q} - \frac{\alpha(1+\epsilon)}{1+\epsilon\alpha}\boldsymbol{q}_{\mathrm{R}}, \tag{A 4}$$

$$\boldsymbol{j}_{\mathrm{D}} = \alpha\boldsymbol{q}_{\mathrm{D}}, \tag{A 5}$$

$$\boldsymbol{j}_{\mathrm{C}} = (1-\alpha)\,\boldsymbol{q}_{\mathrm{C}}, \tag{A 6}$$

$$\boldsymbol{j} = \boldsymbol{j}_{\mathrm{D}} + \boldsymbol{j}_{\mathrm{C}}, \tag{A 7}$$

$$\boldsymbol{j} = \boldsymbol{q} - \epsilon\frac{\alpha(1-\alpha)}{1+\epsilon\alpha}\boldsymbol{q}_{\mathrm{R}}, \tag{A 8}$$

$$\boldsymbol{j}_{\mathrm{D}} = \alpha\boldsymbol{j} + \alpha(1-\alpha)\,\boldsymbol{q}_{\mathrm{R}}, \tag{A 9}$$

$$\boldsymbol{j}_{\mathrm{D}} = \alpha\boldsymbol{q} + \frac{\alpha(1-\alpha)}{1+\epsilon\alpha}\boldsymbol{q}_{\mathrm{R}}, \tag{A 10}$$

$$\boldsymbol{j}_{\mathrm{C}} = \frac{1-\alpha}{\alpha}\boldsymbol{j}_{\mathrm{D}} - (1-\alpha)\,\boldsymbol{q}_{\mathrm{R}}. \tag{A 11}$$

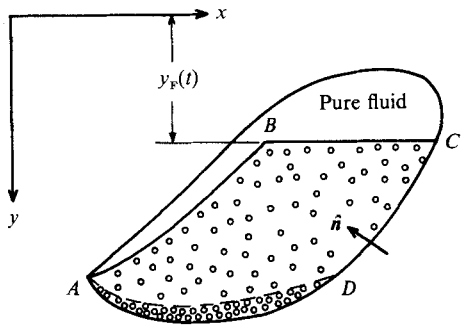

FIGURE 11. Schematic section in a mixture of heavy particles settling in the y-direction in compliance with PNK theory.

Appendix B. Results of the PNK theory

Refer to figure 11. Assume that the pure fluid layer and the opposite sediment layer on the inclined walls are thin, $\alpha = \alpha(t)$, the interface BC is perpendicular to $\hat{\boldsymbol{y}}$ and the relative velocity $\boldsymbol{v}_D - \boldsymbol{v}_C$ is

$$\boldsymbol{v}_R = v_R \hat{\boldsymbol{y}}. \tag{B 1}$$

Let $V_m(t)$ be the instantaneous volume of mixture (bounded by $ABCDA$) which contains the total subvolume V_D of dispersed particles. The volumetric settling rate is given by:

$$-\frac{dV_D}{dt} = -\oint_{ADCBA} \boldsymbol{j}_D \cdot \hat{\boldsymbol{n}}\, dA = -\int_{ADC} \boldsymbol{j}_D \cdot \hat{\boldsymbol{n}}\, dA$$

$$= -\int_{ADC} [\alpha \boldsymbol{j} + \alpha(1-\alpha)\boldsymbol{v}_R] \cdot \hat{\boldsymbol{n}}\, dA = \alpha(1-\alpha)\int_{ADC} v_R |\hat{\boldsymbol{n}} \cdot \hat{\boldsymbol{y}}|\, dA, \tag{B 2}$$

where the boundary conditions $\boldsymbol{j}_D \cdot \hat{\boldsymbol{n}} = 0$ on ABC, $\boldsymbol{j} \cdot \hat{\boldsymbol{n}} = 0$ on the sediment and solid walls, and equations (A 7) and (B 1) have been used.

Since $V_D = \alpha V_m$ it follows with the aid of (B 2)

$$\frac{dV_m}{dt} = \frac{1}{\alpha}\left(\frac{dV_D}{dt} - \frac{d\alpha}{dt} V_m\right) = -(1-\alpha)\int_{ADC} v_R |\hat{\boldsymbol{y}} \cdot \hat{\boldsymbol{n}}|\, dA - \frac{1}{\alpha}\frac{d\alpha}{dt} V_m. \tag{B 3}$$

Letting A_{BC} denote the area of the front interface perpendicular to $\hat{\boldsymbol{y}}$, it is observed that

$$\frac{dV_m}{dt} = -A_{BC}\frac{dy_F}{dt}. \tag{B 4}$$

Consequently, (B 3)–(B 4) give

$$\frac{dy_F}{dt} = \frac{1}{A_{BC}}\left[(1-\alpha)\int_{ADC} v_R |\hat{\boldsymbol{y}} \cdot \hat{\boldsymbol{n}}|\, dA + \frac{1}{\alpha}\frac{d\alpha}{dt} V_m\right]. \tag{B 5}$$

In gravitational settlers v_R and α are usually constant. For a two-dimensional tank of width l one therefore obtains:

$$\left(-\frac{dV_D}{dt}\right) = \alpha(1-\alpha) v_R\, l[x_C(t) - x_A], \tag{B 6}$$

$$\frac{dy_F}{dt} = (1-\alpha) v_R \left[\frac{x_C(t) - x_A}{x_C(t) - x_B(t)}\right]. \tag{B 7}$$

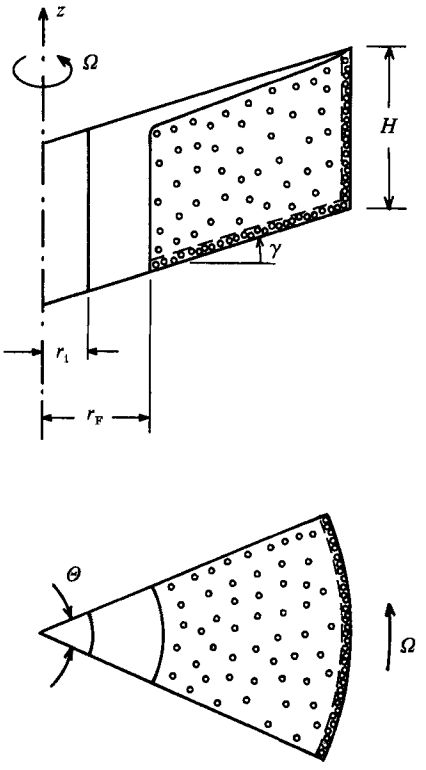

FIGURE 12. Schematic view of a rotating container for illustrating the centrifugal analog of PNK theory; $0 < \Theta \leqslant 2\pi$.

Here $x_B(t)$ and $x_C(t)$ are approximated by the points cut by the horizontal interface on the given walls of the container. For the configuration of figure 1 this reads

$$\left(-\frac{\mathrm{d}V_D}{\mathrm{d}t}\right) = \alpha(1-\alpha)\, v_R\, l \frac{1}{\cos\gamma}[b + h\sin\gamma], \tag{B 8}$$

$$\frac{\mathrm{d}h}{\mathrm{d}t} = -(1-\alpha)\, v_R\left(1+\frac{h}{b}\sin\gamma\right). \tag{B 9}$$

(The enhancement follows from comparison to $\gamma = 0$.)

In the centrifugal case, x and y correspond to the axis of rotation and radial coordinate r, respectively. Moreover, $v_R \equiv \boldsymbol{q}_R \cdot \hat{\boldsymbol{r}}$ is given by (2.8) and $\mathrm{d}\alpha/\mathrm{d}t = -2\Phi(\alpha)$ via (2.9). The consequences of (B 2) and (B 5) usually require numerical (but still straightforward) solution. For example, for the container of figure 12 one gets, in dimensionless form,

$$\left[-\frac{\mathrm{d}V_D}{\mathrm{d}t}\right] = \Phi(\alpha)\,\Theta H\left[1+\frac{1}{3H}\tan\gamma(1-r_F^3)\right], \tag{B 10}$$

$$\frac{\mathrm{d}r_F}{\mathrm{d}t} = \frac{\Phi(\alpha)}{\alpha}\frac{1}{r_F}\left[r_F^2+\frac{1}{3H}\tan\gamma(1-r_F^3)\right]. \tag{B 11}$$

Further approximations for the dilute case ($\Phi(\alpha) \approx \alpha \approx \alpha(0)\,\mathrm{e}^{-2t}$; $\alpha(0) \ll 1$) and initial state ($r_{\mathrm{F}}^3 \ll 1$) yields:

$$\Delta V_{\mathrm{d}} \approx \tfrac{1}{2}\Theta H\alpha(0)\left[1+\frac{1}{3H}\tan\gamma\right](1-\mathrm{e}^{-2t}), \tag{B 12}$$

$$r_{\mathrm{F}}^2 \approx \left(r_{\mathrm{i}}^2+\frac{1}{3H}\tan\gamma\right)\mathrm{e}^{2t}-\frac{1}{3H}\tan\gamma, \tag{B 13}$$

where ΔV_{D} represents the settled volume of dispersed particles.

REFERENCES

Acrivos, A. & Herbolzheimer, E. 1979 Enhanced sedimentation in settling tanks with inclined walls. *J. Fluid Mech.* **92**, 435–457.

Amberg, G., Dahlkild, A. A., Bark, F. H. & Henningson, D. S. 1986 On time-dependent settling of a dilute suspension in a rotating conical channel. *J. Fluid Mech.* **166**, 473–502.

Amberg, G. & Greenspan, H. P. 1987 Boundary layers in a sectioned centrifuge. *J. Fluid Mech.* **181**, 77–97.

Greenspan, H. P. 1968 *The Theory of Rotating Fluids.* Cambridge University Press.

Greenspan, H. P. 1983 On centrifugal separation of a mixture. *J. Fluid Mech.* **127**, 91–101.

Greenspan, H. P. & Ungarish, M. 1985*a* On the enhancement of centrifugal separation. *J. Fluid Mech.* **157**, 359–373.

Greenspan, H. P. & Ungarish, M. 1985*b* On the centrifugal separation of a bulk mixture. *Intl J. Multiphase Flow* **11**, 825–835.

Ishii, M. 1975 *Thermo-fluid Dynamic Theory of Two-phase Flow.* Paris: Eyrolles.

Ishii, M. & Zuber, N. 1979 Drag coefficient and relative velocity in bubbly, droplet of particulate flows. *AIChE J.* **25**, 843–846.

Moore, D. W. & Saffman, P. G. 1969 The structure of free vertical shear layers in a rotating fluid and the motion produced by a slowly rising body. *Phil. Trans. R. Soc. Lond.* A **264**, 597–633.

Schaflinger, U., Köppl, A. & Filipczak, G. 1986 Sedimentation in cylindrical centrifuges with compartments. *Ing. Arch.* **56**, 321–331.

Schneider, W. 1982 Kinematic-wave theory of sedimentation beneath inclined walls. *J. Fluid Mech.* **120**, 323–346.

Ungarish, M. 1986 Flow of a separating mixture in a rotating cylinder. *Phys. Fluids* **29**, 640–646.

Ungarish, M. 1988 Two-fluid analysis of centrifugal separation in a finite cylinder. *Intl J. Multiphase Flow* **14**, to appear.

Ungarish, M. & Greenspan, H. P. 1984*a* On the radial filling of a rotating cylinder. *J. Fluid Mech.* **141**, 97–107.

Ungarish, M. & Greenspan, H. P. 1984*b* On centrifugal separation of particles of two-different sizes. *Intl J. Multiphase Flow* **10**, 133–148.